Structure and Electric Properties of Sn_N Clusters ($N = 6-20$) from Combined Electric Deflection Experiments and Quantum Theoretical Studies

Sascha Schäfer,*,† Behnam Assadollahzadeh,‡ Max Mehring,† Peter Schwerdtfeger,‡ and Rolf Schäfer†

Eduard-Zintl-Institut für Anorganische and Physikalische Chemie, Technische Universität Darmstadt, Germany, and Centre of Theoretical Chemistry and Physics, The New Zealand Institute for Advanced Study, Massey University (Auckland Campus), Private Bag 102904, North Shore City, 0745 Auckland, New Zealand

Received: April 9, 2008; Revised Manuscript Received: September 15, 2008

Electric deflection experiments have been performed on neutral Sn_N clusters ($N = 6-20$) at different nozzle temperatures in combination with a systematic search for the global minimum structures and the calculation of the dielectric properties based on density functional theory. For smaller tin clusters ($N = 6-11$), a good agreement between theory and experiment is found. Taking theoretically predicted moments of inertia and the body fixed dipole moment into account permits a quantitative simulation of the deflected molecular beam profiles. For larger Sn_N clusters ($N = 12-20$), distinct differences between theory and experiment are observed; i.e., the predicted dipole moments from the quantum chemical calculations are significantly larger than the experimental values. The investigation of the electric susceptibilities at different nozzle temperatures indicates that this is due to the dynamical nature of the tin clusters, which increases with cluster size. As a result, even at the smallest nozzle temperature of 40 K, the dipole moments of Sn_{12-20} are partially quenched. This clearly demonstrates the limits of current electric deflection experiments for structural determination and demonstrates the need for stronger cooling of the clusters in future experiments.

1. Introduction

For a better understanding of the size-dependent properties of isolated homoatomic clusters in the gas phase, a structural characterization is an important prerequisite. For charged clusters, mass-selective vibrational spectroscopy in combination with quantum theoretical approaches has led to a decisive breakthrough.[1] In addition, electron diffraction on charged clusters in an ion trap gives direct access to structural data.[2,3] Moreover, the investigation of drift mobilities[4−6] and surface-induced dissociation of mass selected cluster ions,[7,8] together with photodissociation studies,[9] allows greater insight into the structure of clusters.

For anions, photoelectron spectroscopy is one of the most powerful tools to investigate the electronic and geometric structure of various clusters.[10] In contrast, the structural characterization of neutral clusters turns out to be more difficult as the mass-selective investigation requires photoionization of these clusters in the (vacuum)-ultraviolet spectral range in an additional step. One may think of the ionization potentials as a probe for the geometric structure of these clusters.[11] This, however, is hardly possible because differences in ionization potentials of different cluster isomers are often too small to be detected experimentally.[12]

Photoelectron spectroscopic investigation of neutral clusters has been conducted only on a few clusters within a coincidence experiment.[13−15] Infrared spectroscopic studies on neutral clusters are also feasible in principle if the experiments performed on the cations are expanded with an additional ionization step. With a tunable free electron laser, first experiments on neutral metal clusters have recently been carried out.[16,17] Multiphoton ionization is also suitable to characterize the structure of clusters,[18] particularly if rotationally resolved absorption spectra are available. But as a rule, this method is limited to small aggregates only. In addition to the spectroscopic approaches mentioned so far, dielectric properties could also be used as a probe for the geometric arrangements of neutral clusters.[19] Here however, measurements of static polarizabilities are again not sensitive enough to discriminate between different isomers.[20,21] In contrast, the formation of dipole moments is strongly affected by the deformation of the clusters from spherical symmetry.[22,23] However, the detection of dipole moments for larger element clusters still remains an experimental challenge.

In the present work we demonstrate that electric deflection experiments together with a systematic quantum theoretical approach are in principle capable of determining the structures of small neutral metal clusters. For this purpose, we have studied neutral Sn_N clusters from $N = 6$ to 20. So far, only ionization potentials[11] and formation enthalpies of the neutral Sn_N clusters are known,[24−26] and only a few theoretical investigations concerning the structures and binding energies of neutral tin clusters are available.[27−32] Therefore, in addition to our deflection experiments we performed a systematic theoretical search for new global minimum structures and determined their static dipole polarizabilities and dipole moments for the first time. In order to verify the calculated structures for cold, rigid tin clusters, we utilized the optimized structures, together with their tensor of inertia and predicted body fixed dipole moments, and simulated the measured molecular beam profiles. This approach permits in principle a quantitative analysis of the deflection experiments.

The paper has the following structure: First, we provide a short overview of the experimental and the quantum theoretical methodology. After a qualitative discussion of the experimental

* Corresponding author, sascha@cluster.pc.chemie.tu-darmstadt.de.
† Technische Universität Darmstadt.
‡ Massey University.

10.1021/jp8030754 CCC: $40.75
Published on Web 11/08/2008

results, we analyze the measured beam profiles within the context of first order perturbation theory. Finally, we cover the simulated molecular beam profiles based on our quantum theoretical calculations in order to validate the obtained structures of the neutral tin clusters in the gas phase.

2. Experimental and Theoretical Methods

2.1. Experimental Methods. An overview of the apparatus used in this work can be found in the literature[33,34] and is therefore only briefly described here. Tin clusters are produced by a pulsed laser vaporization source.[33] Here, a tin rod is irradiated with the focused light from a Nd:YAG laser, forming a small amount of a plasma. The plasma is then cooled down in a flow of helium gas, which subsequently condenses to form clusters. The helium−tin cluster mixture is then expanded through a nozzle into a high-vacuum apparatus, thereby producing a supersonic beam of Sn_N clusters. The nozzle has a length of 61 mm and a diameter of 3 mm. The leading 25 mm of the nozzle can be cooled down to 40 K by utilizing a helium refrigerator, thus enabling further reduction of the clusters' kinetic energy in the beam and further cooling of their internal degrees of freedom. In the present work, experiments at nozzle temperatures between 40 and 100 K were performed. The molecular beam is subsequently narrowed using a double skimmer and is passed through a chopper, which enables measurement of cluster velocities in the molecular beam.[35] After passing two collimators, the molecular beam reaches the inhomogeneous electric field. The electric field used in the experiment is the electric analogue of the so-called "two-wire-magnetic-field" first developed by Rabi and co-workers.[36] This setup yields a constant product of the electric field and its gradient throughout the dimensions of the molecular beam. The experimental setup of the deflection electrodes is similar to the one reported by Bederson et al.[37,38] The distance between the two electrodes is 1.5 mm. The strongest electric field generated in this work is 2×10^7 V/m. About 1200 mm downstream of the deflection unit, the clusters are ionized using an excimer laser (7.89 eV) after passing a slit of width 400 μm. Its position can be varied with an accuracy of 2 μm. Ionized clusters reach then the acceleration zone of the time-of-flight (TOF) mass spectrometer, are deflected perpendicularly to the molecular beam axis with a strong voltage pulse applied to the meshes of the acceleration unit, and are finally detected by an Even-cup.[39]

The cluster polarizabilities and dipole moments are determined using the barium atom as a calibrant with an accurately determined polarizability of 39.7 ± 3.2 Å^3.[34,40] Therefore, the absolute values of all the reported polarizabilities and dipole moments have an uncertainty of about 8%. The statistical uncertainties due to the measurement of the beam profiles and cluster velocities are indicated as error bars.

2.2. Theoretical Methods. The predicted singlet and triplet global minimum structures of tin clusters ranging from 6 up to 20 atoms were obtained using a recently developed genetic algorithm code.[21] The initial populations of typically 10−15 different structures consisted of randomly generated structures, predicted Lennard-Jones global minima, and recently published low-lying minima structures for tin[28] and silicon clusters.[41,42] The search for the global minimum of a specific cluster was performed in combination with an ultrasoft pseudopotential for tin within the plane-wave method, leaving the $5s^2\,5p^2$ electrons in the valence space and applying the local spin-density approximation as implemented in the VASP program package.[43] The cutoff energy for the plane-wave expansion was set to be 6 Ry. The clusters were placed in a cubic cell with side lengths of 16 Å constrained to periodic boundary conditions. During the global optimization, the cell was dynamically adapted, ensuring a distance of greater than 8 Å between the clusters. Typically 8−10 of the thus obtained energetically lowest-lying isomers were then further relaxed to their local minima applying Los Alamos pseudopotentials and corresponding basis sets.[44] Depending on the energy distribution, two to four of the energetically lowest-lying true minima structures obtained were then further optimized using a more accurate Stuttgart small-core energy-consistent relativistic pseudopotential together with an extensive valence basis set for tin[45,46] and the B3P86 hybrid functional as suggested by Becke[47] and Perdew.[48] No symmetry constraints were applied during the optimization procedure. Finally, harmonic vibrational frequencies were computed to ensure that the relaxed geometries are true local minima on the potential energy surface. To find the best DFT functional reproducing accurately the mean static dipole polarizability of the tin clusters, the polarizability of the ^{3}P ground state of the tin atom was calculated at the coupled cluster level of theory, CCSD(T), from an uncontracted and extended Stuttgart valence basis set[45,46] with the respective energy-consistent relativistic pseudopotential which gave for the isotropic polarizability $\alpha = 8.04$ Å^3. We tested a number of different density functionals, with the B3P86 functional yielding the smallest deviation from the coupled cluster value, i.e., $\alpha = 8.07$ Å^3.[49] Hence this functional was chosen for all final calculations.

3. Results and Discussion

3.1. Structural Data. Figure 1 depicts the predicted global minima and close lying low-energy isomers of the singlet states of Sn_{6-20} with relative energy differences of up to about 0.5 eV. Interestingly, for these clusters the putative global minima with triplet spin state are at least 0.35 eV higher in energy than the corresponding singlet global minimum. Quintet spin states were also investigated for a variety of different structures of Sn_{2-7} and were found to lie even higher in energy by 1−2 eV. Thus, they are not expected to play an important role in the characterization of the global minima of Sn_{6-20} and will not appear in experiments at low temperatures. Relative energies, point group symmetries, static electric response, dipole moments, and moments of inertia are shown in Table 1. We also include Ray's asymmetry parameter κ[50] for asymmetric tops defined as

$$\kappa = \frac{2/I_b - 1/I_a - 1/I_c}{1/I_a - 1/I_c} \quad (1)$$

with I being the principal moments of inertia. $\kappa = 1$ corresponds to an oblate, $\kappa = -1$ to a prolate, and $\kappa \approx 0$ to a strongly asymmetric rotor.

In accordance with the literature,[27,28] the hexamer displays a distorted octahedral structure (**6s0**), Sn_7 a pentagonal bipyramidal structure (**7s0**), and the octamer is an edge-capped pentagonal bipyramid (**8s0**). The nonamer ground-state structure is a distorted singlet bicapped pentagonal bipyramid (**9s0**) and more stable by 0.43 eV than the tricapped trigonal prism (TTP) in the triplet state. This contradicts recent work,[28] which claims that the TTP structure of Sn_9 is the global minimum. We note that even using the Los Alamos pseudopotentials and corresponding basis sets the energetic preference for the singlet state compared to the triplet state is 0.53 eV for the **9s0** structure and 0.27 eV for the TTP structure. The global minimum of Sn_{10} clearly shows the trigonal prism motif and represents a symmetrical tetracapped derivative of it (**10s0**). The energetically

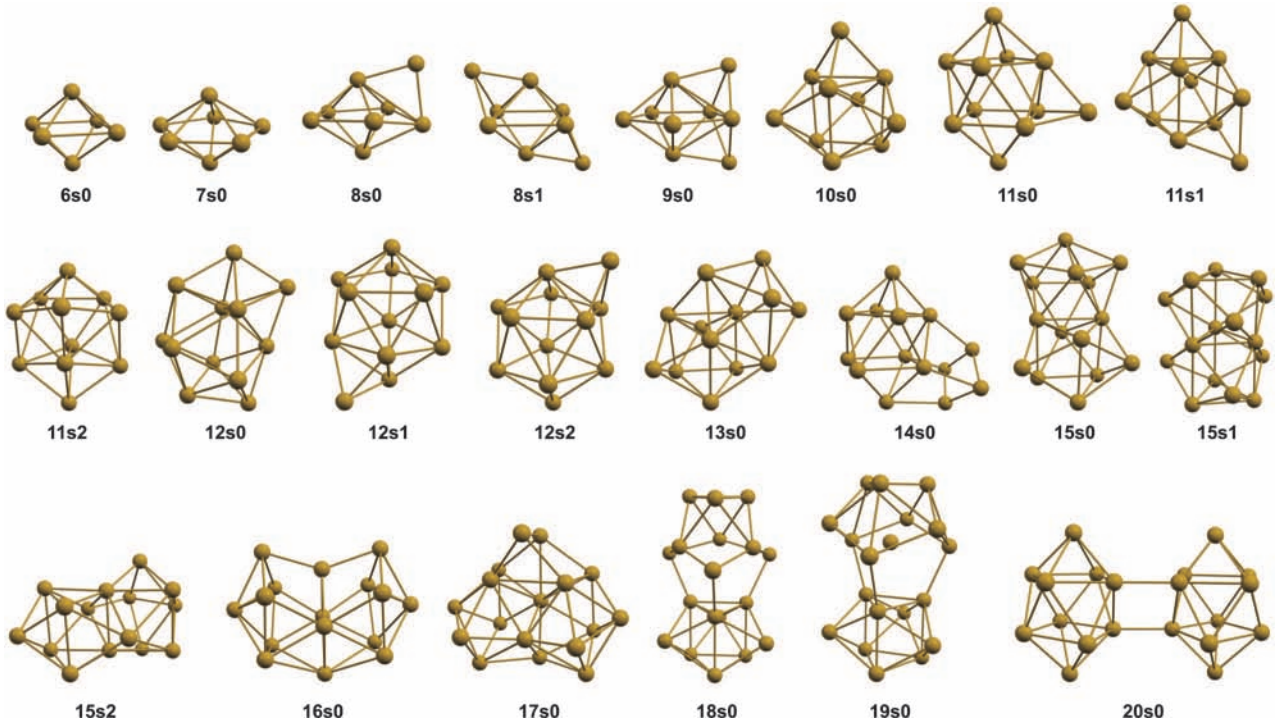

Figure 1. Calculated global minima and few energetically low-lying isomers of Sn_N ($N = 6-20$).

TABLE 1: Point Group Symmetries, Relative Energies $\Delta\epsilon$ (in eV), Isotropic Dipole Polarizabilities α_{iso} per Atom (in Å^3), Experimental Dipole Polarizabilities α (in Å^3), Dipole Moments μ (in D), Principal Moments of Inertia $I_{a,b,c}$ (in 10^{-44} kg·m^2), and Ray's Asymmetry Parameter κ of the Calculated Global Minima Structures and Few Energetically Low-Lying Isomers of Sn_N ($N = 6-20$) as Depicted in Figure 1[a]

isomer	symmetry	$\Delta\epsilon$	α_{iso}	α_{exp}	$\lvert\mu\rvert$	μ_a	μ_b	μ_c	I_a	I_b	I_c	κ
6s0	D_{4h}	0	7.26	7.3 ± 0.4	0	0	0	0	3.26	3.26	4.27	1
7s0	D_{5h}	0	7.11	8.3 ± 0.4	0	0	0	0	4.18	4.18	6.40	1
8s0	C_s	0	7.31	15.1 ± 0.3	0.57	0.33	0	0.46	5.01	6.76	7.81	−0.45
8s1	C_{2h}	0.19	7.49	15.1 ± 0.3	0	0	0	0	4.06	8.09	8.76	−0.86
9s0	C_{2v}	0	7.20	10.2 ± 0.4	0.21	0.21	0	0	6.68	8.69	8.89	−0.86
10s0	C_{3v}	0	7.02	14.7 ± 0.3	0.63	0.63	0	0	9.71	10.11	10.11	−1
11s0	C_s	0	7.14	30.5 ± 0.5	1.59	1.39	0.78	0	10.04	11.53	13.13	−0.10
11s1	C_s	0.02	7.27	30.5 ± 0.5	0.54	0.45	0.29	0	9.59	12.79	13.38	−0.77
11s2	C_s	0.10	7.15	30.5 ± 0.5	1.31	1.31	0	0.08	10.06	11.75	12.91	−0.31
12s0	C_1	0	7.26	30.5 ± 0.3	2.25	2.11	0.79	0.07	10.75	14.47	17.12	−0.38
12s1	C_1	0.06	7.28	30.5 ± 0.3	1.40	1.30	0.14	0.51	10.42	15.27	16.76	−0.68
12s2	C_1	0.08	7.20	30.5 ± 0.3	1.13	1.07	0.04	0.35	11.39	14.43	15.84	−0.50
13s0	C_1	0	7.28	26.8 ± 1.0	0.75	0.70	0.13	0.23	11.61	18.81	19.41	−0.91
14s0	C_s	0	7.35	20.2 ± 0.5	0.98	0.91	0.36	0	13.64	22.14	22.50	−0.95
15s0	C_{2v}	0	7.30	15.5 ± 0.5	0.07	0	0.01	0.07	14.70	24.61	26.00	−0.85
15s1	D_{3h}	0.09	7.12	15.5 ± 0.5	0	0	0	0	16.21	22.69	22.69	−1
15s2	C_s	0.25	7.34	15.5 ± 0.5	0.85	0.85	0	0	14.32	25.40	27.16	−0.85
16s0	C_{2v}	0	7.29	15.8 ± 0.3	0.86	0.86	0	0	16.96	27.56	29.48	−0.81
17s0	C_s	0	7.27	18.4 ± 1.2	0.93	0	0.77	0.52	21.62	27.02	31.14	−0.31
18s0	C_{3v}	0	7.52	13.3 ± 0.3	1.94	1.94	0	0	19.07	40.53	40.53	−1
19s0	C_{3v}	0	8.01	19.1 ± 0.3	0.97	0.97	0	0	20.96	44.10	44.10	−1
20s0	C_s	0	8.00	15.9 ± 1.0	0.13	0	0.11	0.06	21.53	58.64	63.36	−0.92

[a] $\mu_{a,b,c}$ are the components of the dipole moment vector in the principal axis system.

lowest-lying structures of Sn_{11-13} are all more stable than the ones previously reported in the literature.[28] We point out that the optimization of an icosahedral Lennard-Jones structure for Sn_{13} yields various distorted versions of it, that are all less stable than **13s0** by around 0.8 eV. Our calculated stacked structures of Sn_{14-16}, **14s0**, **15s0**, and **16s0** have been reported previously as the global minimum structures.[28] The predicted global minimum of Sn_{17}, **17s0**, adopts a more spherical structure rather than the prolate ones for the smaller clusters. The structure of Sn_{17} reported by Majumder et al.[28] is less stable than **17s0** by 0.22 eV. The predicted global minima for the 18, 19, and 20 atom clusters are stacked prolate structures, each displaying at least one trigonal prism motif. **18s0** is identical to that found in the literature,[28] while the structures for Sn_{19} and Sn_{20} represent more stable distorted versions. **19s0** consists of a distorted tricapped trigonal prism prolately connected to a distorted tetracapped trigonal prism. The structure **20s0** is based on two identical doubly capped quadratical antiprisms twisted by 180° with respect to each other. Interestingly, all of the proposed global minima between $N = 6$ and 20, except for Sn_6 and Sn_7,

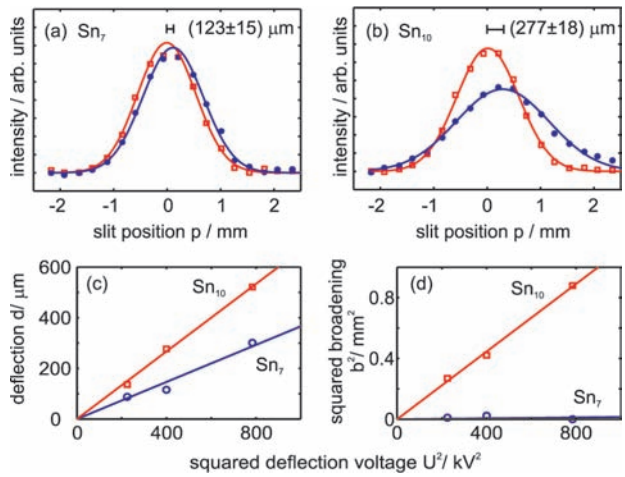

Figure 2. (a, b) Molecular beam profiles of Sn_7 and Sn_{10} with (blue dots) and without (red squares) applied deflection voltage $U = 20$ kV at a nozzle temperature of $T_N = 40$ K. As a guide, Gaussian functions are fitted to the beam profiles. For Sn_7 only a deflection of the molecular beam is visible, whereas for Sn_{10} both a deflection and broadening are observed. (c, d) The beam deflection and squared broadening showing a quadratic dependence on the applied voltage U (see also Supporting Information).

belong to molecular point groups, which do not exclude permanent dipole moments.

3.2. Electric Deflection Experiments. Molecular beam deflection profiles for Sn_7 and Sn_{10} are shown in Figure 2 for a nozzle temperature of 40 K. The beam broadening observed for Sn_{10}, in contrast to Sn_7, clearly demonstrates the existence of a permanent dipole moment, while most of the other tin clusters display smaller but detectable beam broadenings. The experimentally observed beam deflection d of a specific cluster size Sn_N cluster is the weighted average over all deflections d_n of the populated quantum states $|n\rangle$ present in the molecular beam experiment[51]

$$d_n = -\frac{A}{mv^2}\frac{\partial E}{\partial z}\frac{\partial \epsilon_n}{\partial E} \tag{2}$$

The deflections d_n depend on the mass m and velocity v of the particle, an apparatus function A, the gradient $\partial E/\partial z$ of the electric field E, and the linear Stark effect, $\partial \epsilon_n/\partial E$. ϵ_n is the energy of the cluster in the quantum state $|n\rangle$. The apparatus function A depends on the geometry of the electrodes generating the inhomogeneous field and the distance between the electric field and the detection of the clusters.[51] As mentioned before, A has been calibrated against the polarizability of the Ba atom.[40] The measured beam profiles therefore depend on molecular properties such as the permanent electric dipole moment and the electric polarizability and also on the thermal distribution, which may be approximately characterized by a rotational and vibrational temperature T_{rot} and T_{vib}.

One simple approach to discuss the measured beam deflection profiles is by perturbation analysis, which is valid in the low electric field limit. Assuming the clusters as rigid, nearly spherical rotors, their stark effect $(\partial \epsilon_n)/(\partial E)$ in the limit of first-order perturbation theory[50,52] is given by

$$\frac{\partial \epsilon_n}{\partial E} = -\mu\frac{KM}{J(J+1)} - \alpha E \tag{3}$$

with the quantum numbers J, K, and M in the usual nomenclature.[50,52] Within a thermal distribution, all quantum states $n = |JKM\rangle$ for a given quantum number J are equally populated, since the rotors are approximated as nearly spherical rotors. The thermal distribution function ρ depends therefore only on the quantum number J, the rotational constant B, and the rotational temperature T_{rot}:

$$\rho_n = \rho_{JKM} = \rho(J) = \frac{\exp\left(\frac{-BJ(J+1)}{k_b T_{rot}}\right)}{\sum_{J=0}^{\infty}\sum_{K=-J}^{J}\sum_{M=-J}^{J}\exp\left(\frac{-BJ(J+1)}{k_b T_{rot}}\right)} \tag{4}$$

By inserting eq 3 in eq 2 and assuming a thermal distribution of quantum states, the mean value $d = \langle d_n \rangle$ of the deflection distribution is obtained:

$$\begin{aligned}\langle d_n\rangle &= \sum_n \rho_n d_n = \sum_{J=0}^{\infty}\sum_{K=-J}^{J}\sum_{M=-J}^{J}\rho(J)\cdot d_{JKM} = \\ &-\frac{A}{mv^2}\frac{\partial E}{\partial z}\sum_{J=0}^{\infty}\sum_{K=-J}^{J}\sum_{M=-J}^{J}\rho(J)\cdot\left(-\mu\frac{KM}{J(J+1)} - \alpha E\right) = \\ &-\frac{A}{mv^2}\frac{\partial E}{\partial z}\sum_{J=0}^{\infty}\rho(J)\sum_{K=-J}^{J}\sum_{M=-J}^{J}\left(-\mu\frac{KM}{J(J+1)} - \alpha E\right) = \frac{A}{mv^2}\frac{\partial E}{\partial z}\alpha E\end{aligned} \tag{5}$$

Similiarly, the variance $b^2 = \langle (d_n - \langle d_n\rangle)^2\rangle$ is given by

$$\begin{aligned}\langle (d_n - \langle d_n\rangle)^2\rangle &= \sum_n \rho_n (d_n - \langle d_n\rangle)^2 \\ &= \sum_{J=0}^{\infty}\sum_{K=-J}^{J}\sum_{M=-J}^{J}\rho(J)\cdot(d_{JKM} - \langle d_{JKM}\rangle)^2 \\ &= \left(\frac{A}{mv^2}\frac{\partial E}{\partial z}\right)^2\sum_{J=0}^{\infty}\sum_{K=-J}^{J}\sum_{M=-J}^{J}\rho(J)\cdot\left(\mu\frac{KM}{J(J+1)}\right)^2 \\ &= \left(\frac{A}{mv^2}\frac{\partial E}{\partial z}\right)^2\sum_{J=0}^{\infty}\rho(J)\sum_{K=-J}^{J}\sum_{M=-J}^{J}\left(\mu\frac{KM}{J(J+1)}\right)^2 \\ &= \left(\frac{A}{mv^2}\frac{\partial E}{\partial z}\right)^2\sum_{J=0}^{\infty}(2J+1)^2\rho(J)\frac{\mu^2}{9} \\ &= \left(\frac{A}{mv^2}\frac{\partial E}{\partial z}\right)^2\frac{\mu^2}{9}\sum_{J=0}^{\infty}(2J+1)^2\rho(J) = \left(\frac{A}{mv^2}\frac{\partial E}{\partial z}\right)^2\frac{\mu^2}{9}\end{aligned} \tag{6}$$

Therefore, in this simple model, the mean value d of the deflection is connected to the polarizability of the clusters, whereas the variance b^2 of the deflections is caused by a nonvanishing permanent dipole moment. In order to extract d and b^2 from the experimental beam profiles, Gaussian functions are adapted to the measured data points. The values of d are obtained from the shift of the maxima of the Gaussians without and with electric field and b from the square root of the difference of the variances.

The polarizabilities and dipole moments per atom α/N and μ/N obtained from such an approach are shown for Sn_N clusters ($N = 6-20$) in Figure 3 for a nozzle temperature T_N of 40 K. The polarizability per atom of a dielectric or metallic sphere with the density and permittivity of bulk α- and β-Sn is also included in Figure 3.[54] Clearly, the polarizabilities of most of the clusters are well above the ideal metallic or dielectric sphere values. Particularly significant are the large values of the apparent polarizability observed for Sn_{11-13}. The increased apparent polarizabilities arise from nonzero permanent dipole

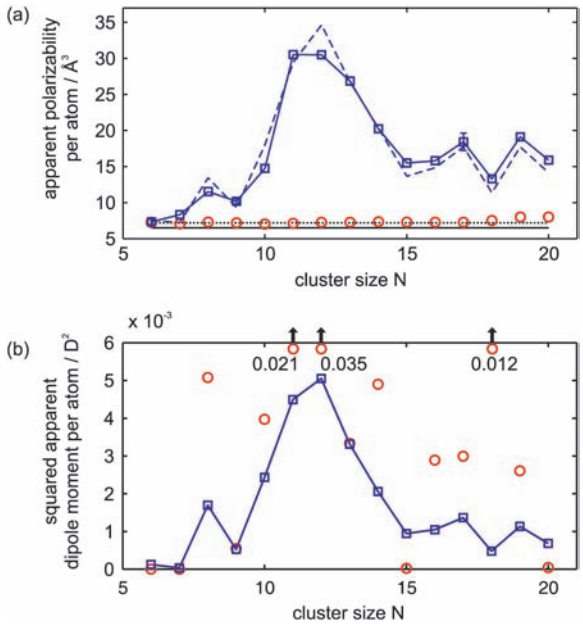

Figure 3. (a) Apparent polarizabilities per atom α/N (blue squares) of Sn_N clusters as obtained from the beam deflection at deflection voltages U between 15 and 28 kV (see Table 1). The experimentally determined apparent polarizabilities are significantly larger than the theoretically predicted polarizabilities (red circles) but can be reproduced, if the dipole moment contribution is incorporated by means of an adiabatic polarization model (broken, blue line) using the experimentally determined permanent dipole moments (see (b)). The polarizability of a sphere with the properties of bulk α- (dotted, black line) and β-Sn (solid, black line) is included for comparison. (b) Squared apparent permanent electric dipole moments per atom $(\mu/N)^2$ (blue squares) as obtained from the voltage-dependent molecular beam broadening. The experimental dipole moments are significantly lower than the theoretically predicted values (red circles, see Table 1) except for $N = 6$, 7, 9, and 13.

contributions to the polarizability (broken, blue line), as predicted by an adiabatic polarization model (see discussion below), which takes the experimentally observed apparent dipole moments into account.

3.3. Apparent Polarizabilities. The calculated isotropic dipole polarizabilities per atom as shown in Table 1 are closer to the value expected for a small dielectric sphere with density and dielectric constant of α-Sn than to the apparent experimental values obtained from the molecular beam deflection. In fact, the deviation is by a factor of 2−4 for most cluster sizes. This is particularly evident as the theoretically predicted polarizabilities per atom for the different isomers of a given cluster size show only variations of less than 10%.

The experimental polarizabilities shown in Figure 3 were calculated using first-order perturbation theory (eq 3). If second-order perturbation theory is used instead, the experimental polarizabilities are only upper limits to the electronic polarizabilities of the clusters, because permanent dipole moments can give a significant contribution to the apparent polarizability due to an adiabatic polarization mechanism.[55,56] Within this model the total polarizability α of a rigid, spherical rotor is divided into two parts. One resulting from a pure electronic polarizability α_e as calculated, and one due to the permanent dipole moment μ

$$\alpha = \alpha_e + \frac{2}{9}\frac{\mu^2}{k_b T_{rot}} \qquad (7)$$

In order to apply the polarization model, we use the experimentally obtained dipole moments from first-order perturbation as a guess to simulate the experimentally observed polarizabilities. For that purpose, the rotational temperature T_{rot} of the ensemble of tin clusters in the molecular beam is needed. To get an idea of the order of magnitude of T_{rot}, we use Sn_{11} as an example. Since the pure electronic contribution to α obtained from a small dielectric sphere of α-Sn amounts to 7.23 Å^3, a rotational temperature of 3.4 K is needed to yield an effective polarizability of 30.5 ± 0.5 Å^3, considering the measured permanent dipole moment of 0.74 D; i.e., the contribution of the permanent dipole moment to the polarizability is 23.3 Å^3. This rotational temperature seems to be reasonable compared to previous molecular beam experiments under similar source conditions.[57] Figure 3 shows the predicted apparent polarizabilities based on the polarization mechanism at a rotational temperature of 3.5 K. Considering the fact that the tin clusters might be nonrigid, nonspherical rotors, the agreement between the experimental values and the polarization model is surprisingly good. The polarization mechanism demonstrates nicely, that for Sn_{11-13} the permanent dipole moments not only give a significant contribution to the measured polarizability but dominate the deflection of the molecular beam. However, it is also evident from Figure 3 that calculated polarizabilities based on the adiabatic polarization model of a spherical rotor cannot explain the measured data quantitatively; e.g., Sn_{10} shows a significantly reduced susceptibility compared to the adiabatic polarization model. Of course, these deviations can be fixed, if a size-dependent rotational temperature is assumed. For example, a rotational temperature of 5.4 K would give an apparent polarizability of Sn_{10} in agreement with Figure 3, but it seems unclear why such temperature differences should occur.[57] The contribution of the permanent dipole moment to the obeserved polarizability α according to eq 7 can be generalized to the case of a symmetric rotor. This gives rise to a prefactor between $(-1/3 + \pi/6)$ and $1/3$ instead of $2/9$ in eq 7, depending on the elongation of the rotor. This might also partially explain the deviations between the adiabatic polarization model and the observed polarizabilities. However, most of the predicted ground-state structures are nonsymmetric rotors ($|k| \neq 1$) and up to now there is no extension of eq 7 for asymmetric tops available.[58]

3.4. Permanent Dipole Moments of Sn_N ($N = 6-11$). The apparent dipole moments per atom, shown in Figure 3, are obtained assuming spherical rigid rotors in the low electric field limit. However, the low electric field limit is possibly already exceeded, since the dipole−field interaction energy, roughly given by $|\vec{\mu}|\cdot|\vec{E}|$, is 2.4 K$\cdot k_b$ for a dipole moment of $\mu = 1$ D at an applied deflection voltage of 15 kV. Moreover, the proposed global minima structures of Sn_{6-20} are asymmetric rotors, except for $N = 6$, 7, 10, 18, and 19. The asymmetry of the structures has two consequences: First, the lower symmetry places no constraints onto the direction of the dipole moment relative to the body principal axes. Second, the asymmetric shape of the inertia tensor strongly alters the rotational motion of the molecule in comparison to a symmetrical rotor.[59] To account for these effects, we used a classical molecular dynamics simulation,[53,60] which treats the molecules as asymmetric rigid rotors and utilized the theoretically predicted dipole moment vectors, isotropic polarizabilities, and moments of inertia. The simulated beam deflection profiles are shown for Sn_{6-11} in Figure 4. For Sn_6, Sn_7, Sn_9, and Sn_{10} the experimental data are nicely reproduced by the theoretical prediction. For Sn_8 and Sn_{11} neither the putative global minima nor the energetically low-lying minima give a reasonable agreement.

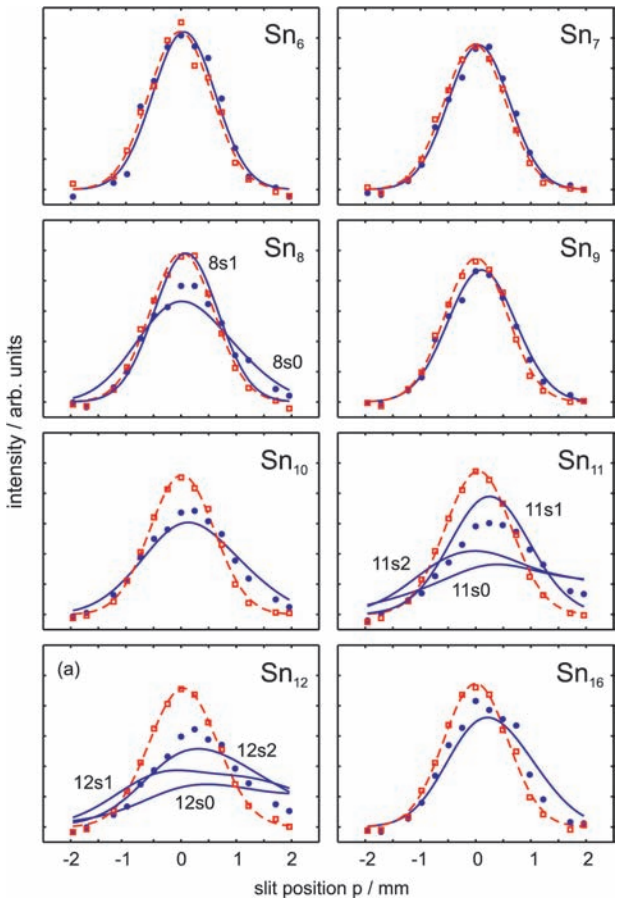

Figure 4. Molecular beam deflection profiles of Sn_6—Sn_{12} and Sn_{16} at a nozzle temperature $T_N = 40$ K and an applied deflection voltage of 15 kV. As a guide to the eye, the undeflected molecular beam profiles (red squares) are approximated by Gaussians (broken, red line). The deflected beam profiles (blue dots) are compared to a molecular dynamics simulation[60] (solid, blue line), which treats the clusters as rigid rotors. The moments of inertia, isotropic polarizabilities, and dipole moments are taken from ab initio calculations (Table 1). A rotational temperature T_{rot} of 3.5 K is assumed, but the results only weakly depend on this actual value.

This can have several reasons. Perhaps, the isomers present in the experiment are not identical to the ones found theoretically, either because the experimental structures are not the global minima due to kinetically controlled growth or the theoretically proposed structures do not represent the true global minima due to incomplete sampling of the configuration space or incorrect energetic ordering of the isomers. Furthermore, one has to keep in mind that the molecular beam deflection critically depends on the orientation and the magnitude of the dipole moment. This indicates that the observed disagreement between theory and experiment could also arise from an inaccurate description of the dipole moment vector by our quantum chemical calculations. However, the good and reasonable description of Sn_9 and Sn_{10} seems to exclude this explanation. Further, a mixture of different isomers may be present in the molecular beam, thus giving rise to observed beam deflections which represent superpositions of different deflected beam profiles. Such an approach is shown in Figure 5 for Sn_8 and Sn_{11} and gives good agreement with the experimental beam profiles assuming that the two energetically lowest isomers contribute to the beam deflection. Especially in the case of Sn_{11} this seems to be a very reasonable assumption since the theoretically predicted energy difference amounts to only 0.02 eV (Table 1). In contrast, for Sn_{12} it is not possible to simulate

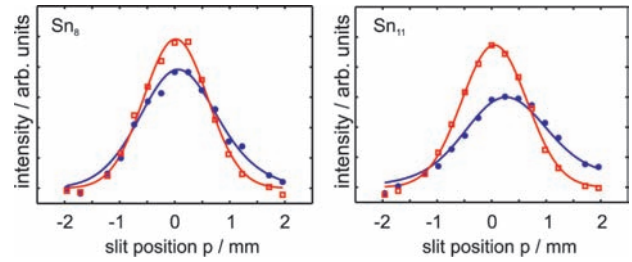

Figure 5. Molecular beam profiles of Sn_8 and Sn_{11} at a nozzle temperature of 40 K with (blue dots) and without (red squares) a deflection voltage of 15 kV. From molecular dynamics simulations, the beam deflection is reproduced well by taking the molecular data from Table 1 into account and further assuming that the molecular beam consists of a mixture of the two lowest isomers **8s0/8s1** and **11s0/11s1**. The population ratio of **8s1** to **8s0** was chosen to be 0.6 and for **11s1** to **11s0** to be 1.5.

the experimental beam profile adequately by taking the two or three low-lying isomers into account.

Two further points important for the analysis of the experimental data need to be addressed. First, it was shown by Abd el Rahim et al.[59] that the rotational motion of rigid asymmetric rotors in external electric fields, contrary to symmetric rotors, can show chaotic behavior depending on the strength of the electric field and the degree of asymmetry of the rotor. Such a behavior would lead to a strong influence of small external perturbations such as electric field inhomogeneities and scattering processes, despite large impact parameters for collision phenomena with background gases. The clusters would thereby lose the memory of their rotational quantum state, leading to a strong reduction of the beam broadening. This could also explain the good agreement between experiment and simulation for the beam deflection of the symmetric rotors **10s0** and the weakly asymmetric rotor **9s0** (see asymmetry parameter in Table 1), in contrast to that for the strong asymmetric rotors **8s0** and **11s0**. The second point deals with the assumption of rigidity. If the clusters interconvert between different isomers on the time scale the particles pass the electric field, typically 200 μs, one would expect a reduced or, in the limiting case, even nonexistent broadening of the molecular beam, i.e., the quenching of the time averaged dipole moment. The rate constant of isomerization will sensitively depend on the vibrational temperature of the clusters, which can be experimentally changed by varying the temperature T_N of the expansion nozzle.

We have therefore investigated the effective dipole moments at different nozzle temperatures between 40 and 100 K. For example, the molecular beam profiles of Sn_{10} are shown in Figure 6a at a nozzle temperature of 100 K and a deflection voltage of 28 kV. Although at 40 K and a deflection voltage of 15 kV a clear broadening of the molecular beam is visible (Figure 4), this broadening almost completely disappeared at 100 K; i.e., the effective dipole moment is close to zero. The deflected molecular beam consistently no longer fits the simulated beam deflection taking the predicted dipole moment, polarizability, and moments of inertia from Table 1 into account. However, even for a simulation assuming a vanishing dipole moment, the experimental results are not properly described, since the transient dipole moments still contribute in a Langevin—Debye mechanism to the effective polarizability and thus enlarge the electronic polarizability.[61] A possible mechanism for the isomerization of Sn_{10} is shown in Figure 6b. It represents a pseudorotation via transition state **10T**, which lies only 0.08 eV higher than **10s0** as obtained from our calculations. This pseudorotation, i.e., the rotation of the dipole moment

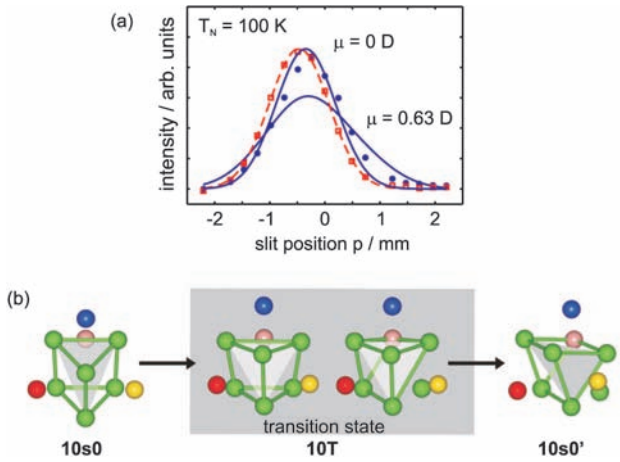

Figure 6. (a) Molecular beam profiles of Sn_{10} with (blue dots) and without (red squares) an applied deflection voltage $U = 28$ kV at a nozzle temperature of 100 K are compared (blue lines) to molecular dynamics simulations taking the theoretically predicted, isotropic polarizability of 7.02 Å^3 and a dipole moment of either 0 or 0.63 D (Table 1) into account. Contrary to the beam deflection at $T_N = 40$ K (Figure 4), the dipole induced broadening is no longer observed at 100 K, which indicates that the cluster cannot be treated as a rigid rotor any more. The apparent polarizability is still enlarged compared to the electronic polarizability due to a Langevin−Debye contribution. (b) A possible mechanism, which quenches the beam broadening of Sn_{10}, is the degenerate isomerization **10s0** → **10s0′** via the transition state **10T**, which lies only 0.08 eV higher in energy than **10s0**. The overall effect of this reaction is a rotation of the dipole moment in the body-fixed coordinate frame. Successive isomerizations result in a vanishing time-averaged dipole moment and a therefore vanishing molecular beam broadening.

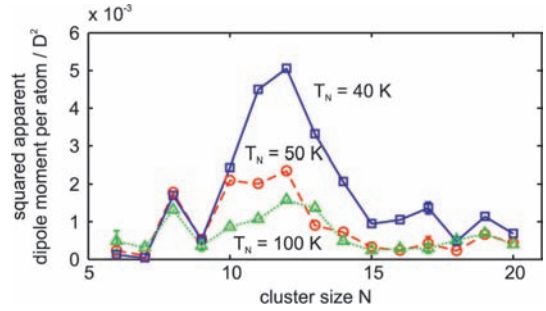

Figure 7. The squared apparent dipole moment obtained from first-order perturbation theory at nozzle temperatures T_N of 40 (blue), 50 (red), and 100 K (green) is shown. For $T_N = 40-50$ K there is no significant change of the apparent dipole moment for Sn_N ($N = 6-10$) but a strong decrease for $N > 10$, which indicates that these clusters cannot be treated as rigid rotors. Increasing the nozzle temperature to 100 K leads also to a decrease of the apparent dipole moment of Sn_{10} (see Figure 6) but also to an increase of the apparent polarizability of Sn_6 and Sn_7. This increase can be explained by a temperature-induced symmetry breaking.[62,63]

vector in the molecular-fixed coordinate frame, clearly demonstrates why the time-averaged dipole moments may be strongly reduced due to the isomerization. Due to the marginal energy difference between the proposed global minimum and the transition state, it is assumed that the pseudorotation is accessible at a time scale of 200 μs.

3.5. Permanent Dipole Moments of Sn_N ($N = 12-20$). For the larger clusters, Sn_{12-20}, there are significant discrepancies between the experimental and theoretical predicted molecular beam deflections, exemplified for Sn_{12} and Sn_{16} in Figure 4. In Figure 7 it is shown, how the experimental size dependent effective dipole moments per atom change with nozzle temperature. For $N = 6-10$ there is almost no change in the effective dipole moment between $T_N = 40$ and 50 K, whereas for $N > 10$ the effective dipole moment is already clearly reduced between $T_N = 40$ and 50 K. This indicates that the molecular beam deflection profiles of Sn_N ($N > 10$) are, at least at $T_N = 50$ K, strongly affected by the flexibility of the structures. Hence it is questionable if these clusters can already be treated as completely rigid bodies at a nozzle temperature of 40 K, thus explaining the poor agreement between experimentally and theoretically predicted beam deflection profiles. In future experiments it is therefore necessary to further cool the clusters down, so that a quantitative comparison with the theoretically proposed structures is possible in this size range. However, in the size range $N = 6-10$ the negligible dependence of the effective dipole moment on the temperature, between $T_N = 40$ and 50 K, suggests that these clusters can be treated as rigid rotors in this temperature regime. Interestingly, the apparent dipole moment of Sn_6 and Sn_7 slightly increase between a nozzle temperature of 50 and 100 K. This indicates, that a temperature-induced symmetry breaking might take place. Similar to what was observed for a carboxylic acid dimer[62] and Na_2C_{60}.[63]

4. Conclusion

We have investigated the dielectric properties of isolated neutral tin clusters in the size range between 6 and 20 atoms. In combination with a systematic theoretical study of the global minima, structures of tin clusters between $N = 6$, 7, 9, and 10 atoms have been confirmed from a quantitative simulation of the measured electric deflection beam profiles by taking calculated moments of inertia and dielectric properties into account. This approach fails for tin clusters with more than 12 atoms, probably because these larger tin clusters are, even at the smallest achieved nozzle temperature of 40 K, still too flexible to be treated as rigid rotors and thus give rise to quenched electric dipole moments. However, by cooling the clusters further, electric deflection experiments together with quantum chemical approaches may be used in the future to determine the structures of larger neutral tin clusters as well. On the other hand, with ever-increasing computer power and the development of almost linear scaling methods, one might be able to simulate accurately the dynamics of small metal clusters at specific temperatures.

Acknowledgment. We acknowledge support from the Deutsche Forschungsgemeinschaft by Grant No. SCHA885/7-1 and -2 and by the Marsden Fund administered by the Royal Society of New Zealand. Sascha Schäfer is grateful to the Fonds der Chemischen Industrie for a scholarship.

Supporting Information Available: Field-induced molecular beam deflection d and broadening b of Sn_6-Sn_{20} at a nozzle temperature $T_N = 40$ K for different deflection voltages. This material is available free of charge via the Internet at http://pubs.acs.org.

References and Notes

(1) Asmis, K. R.; Sauer, J. *Mass Spectrom. Rev.* **2007**, *26*, 542.
(2) Xing, X.; Danell, R. M.; Garzón, I. L.; Michaelian, M. N.; Blom, M. N.; Burns, M. M.; Parks, J. H. *Phys. Rev. B* **2005**, *72*, 081405(R).
(3) Schooss, D.; Blom, M. N.; Parks, J. H.; v. Issendorff, B.; Haberland, H.; Kappes, M. N *Nano Lett.* **2005**, *5*, 1972.
(4) Shvartsburg, A. A.; Jarrold, M. F. *Phys. Rev. A* **1999**, *60*, 1235.
(5) Shvartsburg, A. A.; Jarrold, M. F. *Phys. Rev. Lett.* **2000**, *85*, 2530.
(6) Breaux, G. A.; Neal, C. M.; Cao, B.; Jarrold, M. F. *Phys. Rev. B* **2005**, *71*, 073410.
(7) Tai, Y.; Murukami, J.; Majumder, C.; Kumar, V.; Mizuseki, H.; Kawazoe, Y. *J. Chem. Phys.* **2002**, *117*, 4317.

(8) Waldschmidt, B.; Turra, M.; Schäfer, R. *Z. Phys. Chem.* **2007**, *221*, 1569.
(9) LaiHing, K.; Wheeler, R. G.; Wilson, W. L.; Duncan, M. A. *J. Chem. Phys.* **1987**, *87*, 3401.
(10) Cui, L.-F.; Wang, L.-M.; Wang, L.-S. *J. Chem. Phys.* **2007**, *126*, 064505.
(11) Yoshida, S.; Fuke, K. *J. Chem. Phys.* **1999**, *111*, 3880.
(12) Liu, B.; Lu, Z.-Y.; Pan, B.; Wang, C.-Z.; Ho, K.-M.; Shvartsburg, A. A.; Jarrold, M. F. *J. Chem. Phys.* **1998**, *109*, 9401.
(13) Becker, J.; Rademann, K.; Hensel, F. *Z. Phys. D* **1991**, *19*, 233.
(14) Kaiser, B.; Rademann, K. *Phys. Rev. Lett.* **1992**, *69*, 3204.
(15) Nagaya, K. *J. Phys. Soc. Jpn.* **2003**, *72*, 501.
(16) Fielicke, A.; Rabin, I.; Meijer, G. *J. Phys. Chem. A* **2006**, *110*, 8060.
(17) Fielicke, A.; Ratsch, C.; v.; Helden, G.; Meijer, G. *J. Chem. Phys.* **2007**, *127*, 234306.
(18) Boguslavskiy, A. E.; Ding, H.; Maier, J. P. *J. Chem. Phys.* **2005**, *123*, 034305.
(19) Knight, W. D.; Clemenger, K.; de Heer, W. A.; Saunders, W. A. *Phys. Rev. B* **1985**, *31*, 2539.
(20) Knickelbein, M. B. *J. Chem. Phys.* **2004**, *120*, 10450.
(21) Assadollahzadeh, B.; Bunker, P. R.; Schwerdtfeger, P. *Chem. Phys. Lett.* **2008**, *451*, 262.
(22) Rayane, D.; Compagnon, I.; Antoine, R.; Broyer, M.; Dugourd, P.; Labastie, P.; L'Hermite, J. M.; Le Padellec, A.; Durand, G.; Calvo, F.; Spiegelmann, F. *J. Chem. Phys.* **2002**, *116*, 10730.
(23) Moro, R.; Rabinovitch, R.; Xia, C.; Kresin, V. V. *Phys. Rev. Lett.* **2006**, *97*, 123401.
(24) Meloni, G.; Schmude, R. W.; Kingcade, J. E.; Gingerich, K. A. *J. Chem. Phys.* **2000**, *113*, 1852.
(25) Bachels, T.; Schäfer, R.; Güntherodt, H.-J. *Phys. Rev. Lett.* **2000**, *84*, 4890.
(26) Bachels, T.; Güntherodt, H.-J.; Schäfer, R. *Phys. Rev. Lett.* **2000**, *85*, 1250.
(27) Lu, Z.-Y.; Wang, C.-Z.; Ho, K.-M. *Phys. Rev. B* **2000**, *61*, 2329.
(28) Majumder, C.; Kumar, V.; Mizuseki, H.; Kawazoe, Y. *Phys. Rev. B* **2001**, *64*, 233405.
(29) Joshi, K.; Kanhere, D. G.; Blundell, S. A. *Phys. Rev. B* **2003**, *67*, 235413.
(30) Chuang, F.-C.; Wang, C.-Z.; Ho, K.-M. *Phys. Rev. B* **2004**, *69*, 165408.
(31) Majumder, C.; Kumar, V.; Mizuseki, H.; Kawazoe, Y. *Phys. Rev. B* **2005**, *71*, 035401.
(32) Krishnamurty, S.; Joshi, K.; Kanhere, D. G.; Blundell, S. A. *Phys. Rev. B* **2006**, *73*, 045419.
(33) Bachels, T.; Schäfer, R. *Rev. Sci. Instrum.* **1998**, *69*, 3794.
(34) Schäfer, S.; Mehring, M.; Schäfer, R.; Schwedtfeger, P. *Phys. Rev. A* **2007**, *76*, 052515.
(35) Maguire, L. P.; Szilagyi, S.; Scholten, R. E. *Rev. Sci. Instrum.* **2004**, *75*, 3077.
(36) Rabi, I. I.; Kellog, J. M. B.; Zacharias, J. R. *Phys. Rev.* **1934**, *46*, 157.
(37) Salop, A.; Pollack, E.; Bederson, B. *Phys. Rev.* **1961**, *124*, 1431.
(38) Schäfer, R.; Woenckhaus, J.; Becker, J. A.; Hensel, F. *Z. Naturforsch., A* **1995**, *50*, 445.
(39) Bahat, D.; Cheshnovsky, O.; Even, U.; Lavie, N.; Magen, Y. *J. Phys. Chem.* **1987**, *91*, 2460.
(40) Schwartz, H. L.; Miller, T. M.; Bederson, B. *Phys. Rev. A* **1974**, *10*, 1924.
(41) Hartke, B. *Theor. Chem. Acc.* **1998**, *99*, 241.
(42) Wang, J.; Wang, G.; Ding, F.; Lee, H.; Shen, W.; Zhao, J. *Chem. Phys. Lett.* **2001**, *341*, 529.
(43) Kresse, G.; Furtmüller, J. *Phys, Rev. B* **1996**, *54*, 11169 Vienna *ab initio* simulation package.
(44) Frisch, M. J. ; Trucks, G. W.; Schlegel, H. B.; Scuseria, G. E.; Robb, M. A.; Cheeseman, J. R.; Montgomery, J. A., Jr.; Vreven, T.; Kudin, K. N.; Burant, J. C.; Millam, J. M.; Iyengar, S. S.; Tomasi, J.; Barone, V.; Mennucci, B.; Cossi, M.; Scalmani, G.; Rega, N.; Petersson, G. A.; Nakatsuji, H.; Hada, M.; Ehara, M.; Toyota, K.; Fukuda, R.; Hasegawa, J.; Ishida, M.; Nakajima, T.; Honda, Y.; Kitao, O.; Nakai, H.; Klene, M.; Li, X.; Knox, J. E.; Hratchian, H. P.; Cross, J. B.; Bakken, V.; Adamo, C.; Jaramillo, J.; Gomperts, R.; Stratmann, R. E.; Yazyev, O.; Austin, A. J.; Cammi, R.; Pomelli, C.; Ochterski, J. W.; Ayala, P. Y.; Morokuma, K.; Voth, G. A.; Salvador, P.; Dannenberg, J. J.; Zakrzewski, V. G.; Dapprich, S.; Daniels, A. D.; Strain, M. C.; Farkas, O.; Malick, D. K.; Rabuck, A. D.; Raghavachari, K.; Foresman, J. B.; Ortiz, J. V.; Cui, Q.; Baboul, A. G.; Clifford, S.; Cioslowski, J.; Stefanov, B. B.; Liu, G.; Liashenko, A.; Piskorz, P.; Komaromi, I.; Martin, R. L.; Fox, D. J.; Keith, T.; Al-Laham, M. A.; Peng, C. Y.; Nanayakkara, A.; Challacombe, M.; Gill, P. M. W.; Johnson, B.; Chen, W.; Wong, M. W.; Gonzalez, C.; Pople, J. A. *Gaussian03, Revision C.02*; Gaussian, Inc.: Wallingford, CT, 2003.
(45) Metz, B.; Stoll, H.; Dolg, M. *J. Chem. Phys.* **2000**, *113*, 2563.
(46) Petersen, K. A. *J. Chem. Phys.* **2003**, *119*, 11099.
(47) Becke, A. D. *J. Chem. Phys.* **1993**, *98*, 5648.
(48) Perdew, J. P. *Phys. Rev. B* **1986**, *33*, 8822.
(49) Thierfelder, C.; Assadollahzadeh, B.; Schwerdtfeger, P.; Schäfer, S.; Schäfer, R. *Phys. Rev. A,* in press.
(50) Townes, C. H.; Schawlow, A. L. *Microwave Spectroscopy*; Dover Publications, Inc.: New York, 1975.
(51) Ramsey, N. F. *Molecular Beam*; Clarendon Press: Oxford, 1956.
(52) Kroto, H. W. *Molecular Rotation Spectroscopy*; Dover Publications, Inc.: Mineola, NY, 2003.
(53) Schäfer, S.; Heiles, S.; Becker, J. A.; Schäfer, R. *J. Chem. Phys.* **2008**, *129*, 044304.
(54) *Handbook of Chemistry and Physics*; Lide, D. R., Ed.; CRC Press: Boca Raton, FL, 2002.
(55) Bertsch, G. F.; Yabana, K. *Phys. Rev. A* **1994**, *49*, 1930.
(56) Schnell, M.; Herwig, C.; Becker, J. A. *Z. Phys. Chem.* **2003**, *217*, 1003.
(57) Pokrant, S. *Phys. Rev. A* **2000**, *62*, 051201.
(58) Bulthuis, J; Becker, J. A.; Moro, R.; Kresin, V. V. *J. Chem. Phys.* **2008**, *129*, 024101.
(59) Abd El Rahim, M.; Antoine, R.; Broyer, M.; Rayane, D.; Dugourd, P. *J. Phys. Chem. A* **2005**, *109*, 8507.
(60) Dugourd, P.; Antoine, R.; Abd El Rahim, M.; Rayane, D.; Broyer, M.; Calvo, F. *Chem. Phys. Lett.* **2006**, *423*, 13.
(61) Dugourd, P.; Antoine, R.; Rayane, D.; Benichou, E.; Broyer, M. *Phys. Rev. A* **2000**, *62*, 011201.
(62) Compagnon, I.; Antoine, R.; Rayane, D.; Broyer, M.; Dugourd, P. *Phys. Rev. Lett.* **2002**, *89*, 253001.
(63) Rabilloud, F.; Antoine, R.; Broyer, M.; Compagnon, I.; Dugourd, P.; Rayane, D.; Calvo, F.; Spiegelmann, F. *J. Phys. Chem. C* **2007**, *111*, 17795.

JP8030754